IRACST – International Journal of Computer Networks and Wireless Communications (IJCNWC), ISSN: 2250-3501
Vol.9, No 2, April – June 2019

Aerodynamic effects of inferior turbinate surgery on nasal airflow - a computational fluid dynamics model

X.B. Chen[1], S.C. Leong[2], H.P. Lee[1], V.F.H. Chong[3], D.Y. Wang[4]
[1] Department of Mechanical Engineering, National University of Singapore, Singapore
[2] Common Cold Centre and Healthcare Clinical Trials, Cardiff School of Biosciences, Cardiff University, Wales, United Kingdom
[3] Department of Diagnostic Radiology, Yong Loo Lin School of Medicine, National University of Singapore, Singapore
[4] Department of Otolaryngology, Yong Loo Lin School of Medicine, National University of Singapore, Singapore

Abstract
In cases when conservative measures have failed to alleviate the symptoms of an enlarged inferior turbinates, surgery to achieve a more desirable outcome may be necessary. The purpose of this research was to use CFD simulations to examine how removal of the inferior turbinates affected nasal aerodynamics.
Methods: Three surgical) resection of the bottom third free edge of the inferior turbinate, 2) excision of the head of the inferior turbinate, and 3) radical inferior turbinate resec- tion. The MRI scans of a healthy human subject were utilized to create the models, and a turbulent flow model was employed for the numerical simulation. Three different turbinate surgeries were performed, and their results were compared to those of a healthy nasal model and one with significant nasal blockage. Findings indicated that the majority of streamlines in a healthy nose traveled down the common meatus next to the inferior and middle turbinates with little to no vortices. The streamlines in the nasopharynx were directed superiorly at greater velocity and enhanced wall shear stress when the inferior turbinate was expanded. Resection of the bottom third resulted in the closest to normal wall shear stress and intranasal pressures of the three simulated surgical procedures. Furthermore, streamlines and turbulence in the airflow improved, however they did not recover to pre-change levels. Nasal airflow obstruction due to atrophic rhinitis was reduced after radical turbinate excision.
After radi- cal turbinate surgery, there is little indication that the inspired air is properly conditioned. Resection of the bottom third of the hypertrophic turbinate yields the greatest improvement in nasal aerodynamics, although even the whole decrease is beneficial. It would be necessary to do comparable research on other participants in order to generalize these findings, given they were based on a single individual's data.

***Key words**: inferior turbinate surgery, airflow pattern, nasal cavity, computational fluid mechan-ics, turbulence*

INTRODUCTION

Nasal obstruction caused by enlarged inferior turbinates is a common presentation in clinical practice. Turbinate reduction surgery may be indicated when conservative treatments such as corticosteroids and antihistamines fail. Reducing the bulki- ness of the inferior turbinates will evidently result in improved nasal airflow. However, nasal aerodynamics is far more com- plex than merely restoring the quantity of air traversing thenasal passages. The evidence base supporting the efficacy of surgical management of the hypertrophic inferior turbinate remains low despite many decades of experience. In a system-
atic review of the literature, Batra et al. [1] reported that there was a paucity of good quality clinical trials evaluating and com- paring between the different surgical techniques for inferior turbinate hypertrophy. Few studies utilized objective measures of nasal airflow such as acoustic rhinometry, rhinomanometry, and rhinoresistometry rendering meta-analysis of surgical out- comes impossible. The current gold standard method to objec- tively assess nasal airflow is rhinomanometry [2]. However, this is not routinely utilised in clinical practice and remains pre- dominantly in rhinology research laboratories.

An area of fluid mechanics known as computational fluid dynamics (CFD) use computer simulations to study and solve fluid-flow-related engineering issues. To model the interaction of fluids and gases with boundary-defined and the three surgical techniques described above. For surfaces, we employ computers to do the necessary computations. Few but increasing rhinology labs are using CFD to model nasal airflow and physiology and predict patient outcomes after surgery (3). If you want to learn more about how air flows through your nose, you may use CFD, which provides a very visual model. In the past, methods like rhinomanometry and Mink box simulations have been unable of doing this. Researchers have used CFD to examine the modifications to nasal airflow brought about by septal deviation (4), septal perforation (5,6), and major sinus surgery (7). While there have been studies published modeling the effects of turbinate surgery, these studies used a model of a normal, healthy nose rather than one with hypertrophy inferior turbinates (8,9).

The primary objective of this research was to use CFD simulations to assess the changes in nasal aerodynamics brought on by inferior turbinate surgery. Researchers evaluated the nasal airflow of patients before and after three different surgical treatments on the hypertrophic inferior turbinate. The goal was to compare the outcomes of various surgical treatments on a hypertrophic turbinate model to the flow pattern of a healthy human patient.

MATERIALS AND METHODS

Overal

In order to conduct this research, we first had to get clearance from our institution's ethics committee. Institutional SOPs are adhered to throughout image capture, 3D reconstruction, mesh grid generation, and computer simulation. the details of which have already been published (4,10), albeit a summary of the method itself is provided here.
We used an MRI image of a healthy volunteer (a 183 cm tall, 80 kg man from China) who did not report any sino-nasal issues to construct a realistic nasal model. Endoscopy and acoustic rhinometry both showed a normal and healthy nasal cavity. Using commercially accessible software like MIMICS 12.1 (The Materilize Group, Leuven, Belgium), Hypermesh 9.0 (Altair Engineering, Bangalore, India), and TGrid 4.0, a three-dimensional picture was rebuilt from the 1.5 mm interval MRI data (ANSYS, Inc., Canonsburg, PA, USA). To make computational meshing of the three-dimensional model more manageable, we smoothed the extremely corrugated surfaces that resulted after digitization (Figure 1A). In a comparatively bigger 3-D nasal cavity, smoothing the border surface will not only aid to reduce computing effort and boost computational efficiency, but it will also have no effect on the primary flow pattern within.
Thereafter, we reduced the minimum cross-sectional area of the inferior turbinate by two-thirds by increasing its circumferential expansion by 2 mm to mimic severe blockage (Figure 1B) (10). Partial (Figures 1C and 1D) and radial (Figures 1E and 1F) inferior turbinate excision were among the surgical procedures modeled (Figure 1E). Excision of the turbinal head in a wedge that tapers inferiorly was modeled, as was resection of the lower one-third free margin of the turbinate (Figure 1C) (Figure 1D).

Computational fluid dynamic simulations

Computational fluid dynamic simulations were performed using Fluent 6.3 (ANSYS, Inc.) for the normal nose, severely obstruct- ed nose

Figure 1. Comparison of the geometry of the nasal cavity. (A) Normalhealthy nose. (B) Enlarged inferior turbinate causing nasal obstruction. (C) Lower third of the inferior turbinate excised. (D) Head of the infe-rior turbinate excised (E) Radical inferior turbinate resection. The fig-ures in the top row represent the three-dimensional image of the respective nasal cavities. Figures in the middle row are the geometricalrepresentation of the nasal cavity in sagittal section. Figures in the bot-tom row represent the view of the nasal cavity at the corresponding coronal section.

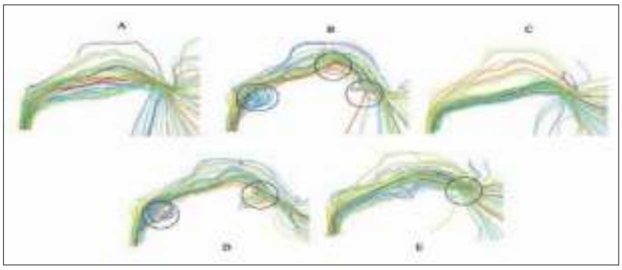

Figure 2. Comparison of the velocity streamlines in the nasal cavity with an inspiratory airflow rate of 17.4 L/min. The vortex areas are cir-cled. (A) Healthy nasal cavity. (B) Enlarged inferior turbinates causingnasal obstruction. (C) Lower third of the inferior turbinate excised. (D)Head of the inferior turbinate excised. (E) Radical inferior turbinate resection.

flow was considered to be incompressible and quasi-steady in the CFD simulations. In order to take into consideration the potential for turbulence, the Reynolds-averaged Navier-Stokes equations were calculated for the turbulent flow using the k-model. In the nasal cavity, the - model approximation is adequate to portray the low levels of whirling and to forecast pressure drop, velocity, and shear stress distributions (11,12). This complicated laminar-transitional-turbulent flow within the nose may be captured using the shear stress transfer (SST) option with transitional flow treatment. The complicated geometry of the nasal cavity is well-suited to the SST model, which combines the - (applied near wall) and - turbulent (applied at the main flow domain) models. At the inlet and outflow borders, we established a turbulence intensity of 6% and a dissipation rate at a dissipation length scale of 0.14 cm. For the purpose of simulating relaxed breathing and rapid sniffing, a boundary condition of a constant flow rate of 17.4, 34.8, and 52.2 L/min at the nasopharynx region was used. While a healthy adult's inspiratory flow rate may vary from 5 L/min to 12 L/min during normal, relaxed breathing, this range was utilised in the experimental setting. With intense physical activity, the flow rate might reach up to 150 L/min (13). Gauge pressure was set equal to zero at the pressure inlet boundary condition at the outside of the face enclosure (atmospheric pressure). To further isolate the impacts of the artificial boundary condition on the simulation findings inside the nasal cavity, it is preferable to have an additional volume of 2,040 cm3 in front of the nose entrance.

Synthesis of Findings

Many formats were used to report the study's findings:
7 total pressure loss from nose to nasopharynx, as well as 1) nasal airflow streamlines, 2) nasal resistance, 3) maximum transient velocity, 4) pressure contours, 5) local Reynolds num-ber, 6) wall shear stress distribution, and its maximum value. The degree of nasal blockage was determined by measuring the resistance of the airflow through the nose, or nasal resis- tance (R = p/Q), with values of Pa s/cm3. During the modeling of turbulent nasal airflow, the greatest value of the transient velocity was found to be localized in the area of the nasal valve. The ratio of inertial forces to viscous forces at a given location is expressed as the local Reynolds number (Re), a dimensionless quantity. At a particular flow condition, it provides a quantitative measure of the significance of the two forces in question. Many types of flow regimes, such as laminar and turbulent flow, may be described by the local Reynolds number. When the local Reynolds number is low enough, viscous forces become the dominating force in the fluid, and the flow becomes laminar. Whereas laminar flow is found at lower local Reynolds numbers and is dominated by gravitational forces, turbulent flow is found at higher local Reynolds numbers and is dominated by inertial forces, leading to random vortices and chaotic flow fluctuations.

RESULTS

The existence of vortices in the flows was seen by plotting the streamlines for the five simulations with varying turbinate conditions (Figure 2). The majority of typical nasal air currents go between the inferior and middle turbinates and the common meatus (Figure 2A). In the nasal valve area, the greatest transient velocity in the healthy model was 3.17 m/s. The streamlines were directed upwards and there were vortices in the nasal valve area, the olfactory groove, and the nasopharynx when the inferior turbinate was expanded artificially to mimic severe obstruct- tion (Figure 2B). This time the peak instantaneous speed was 5.59 meters per second. When one-third of the inferior turbinate was removed, airflow was primarily redirected along the floor of the nasal cavity and the lower part of the common meatus (Figure 2C), with a maximum transient velocity of 2.50 m/s; fewer streamlines flowed in the supe- rior part of the nasal cavity compared to a healthy nose. After having the head of the inferior turbinate removed, the vortex in the olfactory groove vanished, but the ones in the nasopharynx and nasal valve area remained (Figure 2D). Maximum transient velocity remained elevated at 4.96 m/s above the long-term average. After a radial turbinectomy, the streamlines were less organized compared to a normal nose, despite the fact that there were less vortices (Figure 2E). The lowest section of the nose was where the haphazard contours were most evident. The peak transient speed was 2.69 meters per second, which is much lower than average.

With an inspiratory flow rate of 17.4 L/min, the nasal resistance of this healthy adult was 0.032 Pa s/cm3. After the head of the infe- rior turbinate was removed, the resistance dropped to 0.115 Pa s/cm3, whereas it was 0.112 Pa s/cm3 in the severely clogged nose. The nasal resis- tance decreased below the normal value after both lower turbinate excision and radical turbinectomy, to 0.025 Pa s/cm3 and 0.026 Pa s/cm3, respectively.

From nostril to nasopharynx, the pressure contours should gradually drop in a healthy nose (Figure 3A). We measured a larger pressure difference at the nasal valve area, just forward of the head of the inferior turbinate. With a normal nose, there would be a pressure differential of 9.28 Pa between the nostril and the nasopharynx. Figure 3B shows that the substantially blocked nose had a pressure difference of 32.48 Pa, but after having the lower one-third of the inferior turbinate removed, the pressure difference dropped to 7.30 Pa. (Figure 3C). While the amount of the pressure drop was reduced, the distribution of pressure contours resembled those seen in a normal nose. Once the inferior turbinate was surgically removed, there was a marginal rise in pressure to 33.38 Pa compared to the severely blocked nose. After radical turbinectomy, nasal airflow is less impeded, hence the pressure difference is lower than usual at 7.71 Pa.

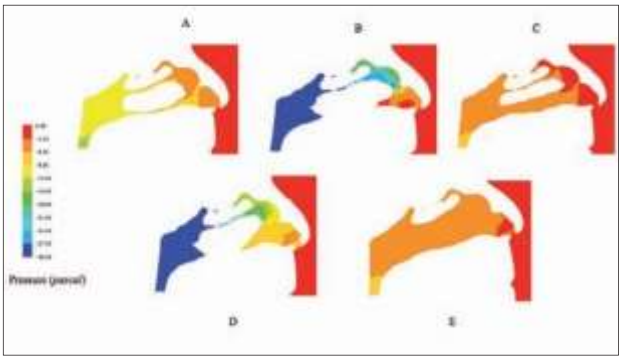

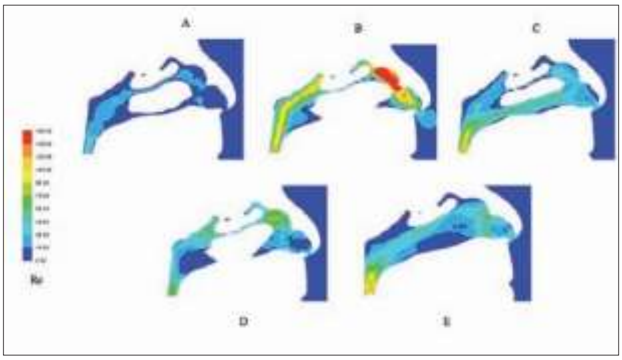

Figure 3. Sagittal cross-section of contour pressure (Pa) at an inspirato- ry flow rate of 17.4 L/min. (A) Healthy nasal cavity. (B) Enlarged infe- rior turbinates causing nasal obstruction. (C) Lower third of the inferi- or turbinate excised. (D) Head of the inferior turbinate excised. (E) Radical inferior turbinate resection.

Figure 4. Comparison of local Reynolds (Re) numbers at an inspiratory flow rate of 17.4 L/min. (A) Healthy nasal cavity. (B) Enlarged inferior turbinates causing nasal obstruction. (C) Lower third of the inferior turbinate excised. (D) Head of the inferior turbinate excised. (E) Radical inferior turbinate resection.

(Figure 3E). The contour pressure distribution remained uni- form throughout the entire nasal cavity.

Figure 4 shows a correlation between the streamline profiles and local Reynolds number profiles from five simulations (Figure 2). The reduced Reynolds number distribution in the nasal cavity of a healthy individual suggested that the airflow was reasonably laminar. As the nasal cavity shrank due to hypertrophy of the inferior turbinates, however, airflow was more likely to be turbulent (with a higher Reynolds number dispersion) (Figure 4B). While turbinectomy does not provide a distribution profile identical to that of a healthy nose, the local Reynolds profile seems to drop and distribute more smoothly after surgery. Airflow in the nasopharynx is substantially more turbulent, as shown by the fact that the local Reynolds number remained high even after turbinectomy.

The absolute Reynolds number was 3.45 at the top of a normal infe- rior turbinate and rose to 67.5 in the unhealthy region.hypertrophic turbinate. Although the Reynolds number reduced with surgical intervention (e.g. 29.7, 46.2 and 27.5 in the cases of lower third, head and radical inferior turbinate resections, respectively), it remained significantly above nor- mal indicating that the area of the resected head in inferior turbinate experienced turbulent airflow.

In the healthy nose, the wall shear stress was generally low to moderate with the maximum stress level at the head of the inferior turbinate of 0.52 Pa (Figure 5A). This area of high stress increased to a maximum of 0.89 Pa when the inferior turbinate was enlarged. The area of high wall shear stress also extended superiorly toward the middle turbinate (Figure 5B). Excision of the lower third of the inferior turbinate appeared to return the wall shear stress profile to near normal distribu-

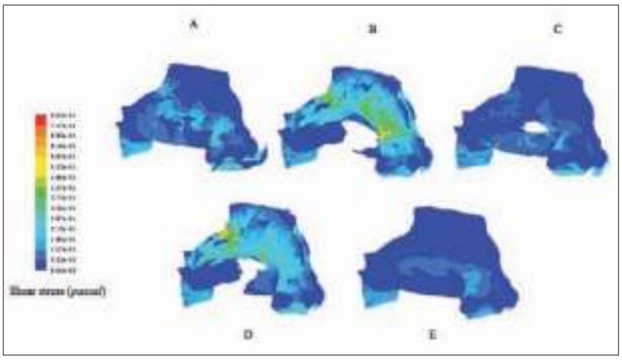

Figure 5. Wall shear stress (Pa) distribution at an inspiratory flow rate of 17.4 L/min. (A) Healthy nasal cavity. (B) Enlarged inferior turbinates causing nasal obstruction. (C) Lower third of the inferior turbinate excised. (D) Head of the inferior turbinate excised. (E) Radical inferior turbinate resection.

Figure 6. Comparison of total pressure loss with different flow rates.

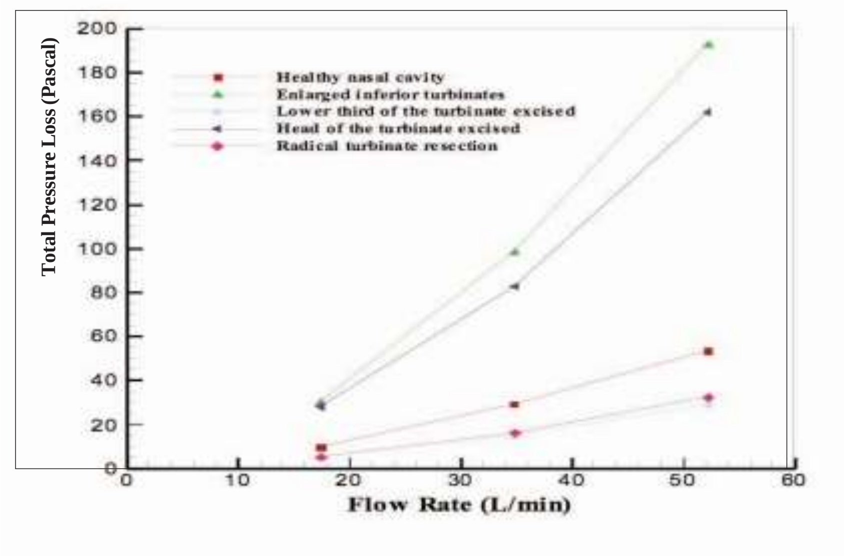

even though the bigger inferior meatus region was now exposed to elevated wall shear stress levels, the area had previously been subjected to a maximum wall shear stress of 0.45 Pa. (Figure 5C). The airflow was simply diverted backwards and the high wall shear stress in the nasopharynx was increased when the turbinate head was removed (Figure 5D). As compared to typical values, the maximum wall shear stress increased by a factor of 2. With a radical turbinectomy, the highest wall shear stress drops to 0.30 Pa, much below the average. In the nasal cavity as a whole, wall shear stress was significantly reduced compared to normal.

For all five scenarios, a higher rate of nasal inspiratory flow resulted in a higher rate of total pressure loss from nose to nasopharynx (Figure 6). This feature was most glaringly noticeable for inferior turbinate hypertrophy, and it only slightly improved following the turbinectomy. After having the bottom third of the turbinates removed and undergoing radical turbinectomy, the patient's airflow and total pressure loss significantly improved.

DISCUSSION

In this research, nasal airflow was analyzed using CFD models before and after partial and whole turbinate reduction surgery. Hypertrophic inferior turbinates were employed in this study's simulations instead of the healthy models that were used in prior research. We think these findings accurately reflect the aerodynamic alterations experienced by those who seek therapy for nasal blockage caused by inferior turbinate hypertrophy. As little is known about nasal airflow after turbinate surgery and how changes in post-operative aerody- namics may lead to problems including atrophic rhinitis, chronic nasal blockage, and hyposmia, the data described here are of therapeutic value.

The Reynolds number profile distribution and wall sheer stress levels looked to be almost normal after conservative turbinate reduction surgery by resecting the lowest one-third. Due to the fact that these factors are associated with air-mucosa contact, which is crucial for air conditioning, the findings provide more support to the idea that the inferior turbinate must be preserved regardless of the surgical approach used in real clinical settings. When the turbinates are surgically removed, it drastically changes the aerodynamics of the nose. After radical turbinate excision, airflow patterns and cross-sectional pressures were similar to those seen in a previously published CFD study of a patient with severe atrophic rhinitis (14). As the air currents inside the atrophic nasal cavity were erratic and turbulent, they made only passing touch with the remaining nasal mucosa along the septum and lateral wall.

Our models agreed with those of Lindemann et al. (8), who modeled the distribution of air temperature in the nasal cavity after radical turbinate excision.

While heat exchange occurred between the sections proximal to the mucosa, the total warming of inspired air was substantially less than that of a typical healthy nose because the center of the airstreams remained chilly throughout the nasal cavity. Because of the desiccating impact of the irregular airflow, symptoms of atrophic rhinitis, such as crusting and fetor, are often seen (15). In addition, in very cold or hot conditions, the lungs may be negatively affected by the inspired air that is not properly conditioned (16).

Grützenmacher et al. (17,18), who conducted Mink box tests using acrylic polymer models of anatomically accurate nasal cavities, likewise found that, in the healthy model, flow was mostly in the common meatus. Radical turbinectomy was also associated with an increase in nasal airflow turbulence and a "unfavourable flow path," as stated by the researchers. Our current calculations are consistent with those of other researchers who have modelled procedures like lateral wall hyperplasia and turbinoplasty. Despite the fact that CFD simulations and the methods utilized in the aforementioned investigations were quite different, the findings showed a strong connection.

In a recent in-depth research, Hörschler et al. explained how crucial the inferior turbinates are for effective HVAC (19) Air conditioning was shown to be more closely connected to nasal geometry during inspiration than expiration when CFD simulations were performed on anatomically correct nasal models. To maintain laminar flow and uniform air velocity distribution throughout the nasal cavity, it was necessary to maintain the inferior turbinate's position inside the nasal valve. In addition, the turbinate's vast surface area allowed for more efficient heat and moisture exchange with the air that was being breathed in (20).

Instead of the laminar flow assumption used in earlier surgical models (9,19), a turbulent flow was introduced in the computational fluid mechanics program by means of the - model with the shear stress transfer (SST). There is little to no noticeable variation in airflow characteristics between the laminar and turbulent models at the low flow rates simulated in this investigation. The use of a turbulent model may in fact be more effective in identifying tiny local vortices. When the SST option is used in conjunction with the - model, the simulations are guaranteed to operate correctly in both the near-wall (where the turbulence is most likely to occur) and far-field areas (more laminar). In most cases, turbulence improves local heat and mass transport by drastically altering local flow patterns. Turbulent flow simulation, which is more computationally intensive than laminar flow modeling, continues to be a difficult and contentious issue (21-,23). For noses with varying nasal physiological symptoms, it is unclear where the laminar, transitional, and turbu- lence areas lie within the complicated nasal cavity. As shown in contemporary nasal models when the inferior turbinates are removed, turbinate reduction improves airway structure.

ture complexity, raises the rate of sudden change in local flow velocity, and maybe enhances the ease with which local turbulence can be induced.

Virtual surgical operations simulated using existing models may not accurately reflect clinical practice. The inferior turbinal enlargement reproduced in this research may not occur in a uniformly circumferential fashion in a clinical setting. The present findings, however, provide the groundwork for further research to assess surgical outcomes using CFD modeling on the hypertrophic turbinate model. Although it is clear that extreme surgery leads in considerably unfavorable flow dynamics, the findings of this research do not necessarily recommend partial or entire turbinate excision as the preferred surgical method. Simulating the current preferred surgical approach to turbinoplasty, as described by Joniau et al. (24), is challenging. Our present approach of resecting the bottom one-third of the turbinates seems to be comparable to the surgical outcome of turbinoplasty, which resulted in the decrease of the inferior turbinate. As a consequence, we think the findings are generalizable to turbinoplasty as well. Gross decrease of the turbinates is likely easier to mimic than other types of tissue volume reduction such as radiofrequency, Coblation®, and laser, which may produce differing aerodynamics. To properly understand how turbinate reduction surgery affects nasal aerodynamics, it would be necessary to compare models using pre- and post-surgical MRI images.

CONCLUSION

This study demonstrated that the nasal flow patterns for inferior turbinate hypertrophy and following turbinate surgery were significantly different from that of a healthy nasal cavity. The existence of vortices induced by turbinate pathology and surgical intervention increases local velocity, shear stress, and total pressure drop values. The implication of these changes is thatthe surgical procedures may need to be carefully planned to minimize impact on the normal functions of the nose. Using CFD techniques, it is now possible to evaluate the effects of inferior turbinate reduction surgery on nasal aerodynamics. It appears that conservative turbinate surgery results in near normal intra-nasal aerodynamics although further studies using real patients are required. The results were based on a single individual and cannot be generalised without similar studies in other subjects.

ACKNOWLEDGEMENT

The authors are grateful to the Ministry of Education, Singapore, for funding via an Academic Research Award (T208A3103). Institutional Review Board approval was obtained for all project-related activities. The Rhinology Journal's 2009–10 Traveling Fellow is Dr. Samuel C. Leong.

REFERENCES

Surgical therapy of adult inferior turbinate hypertrophy: a systematic review of the evidence. Batra P.S., Seiden A.M., and Smith T.L. 2009; 119:1819-1827 Laryngoscope.

Congestion in the nose: causes, assessment, and treatments. Davis SS, Eccles R. Essential facts for the medical professional. Journal of the American Academy of Otolaryngology-Head and Neck Surgery 2004;29:659-666.

Authors: Leong SC, Chen XB, Lee HP, Wang DY. Computational fluid dynamics research with implications for nasal breathing. Rhinology, 48 (2010), pp. 139–145.

Wang DY, Lee HP, Chen XB, and Hin VF. A computational fluid dynamics model of the impact of septal deviation on nasal airflow assessment. Laryngoscope 119(9):1730-1736, 2009.

Research by Pless, Keck, Wiesmiller, et al. Airflow and temperature distribution during inspiration in a model nose with a perforated septum numerically simulated. Publication information: American Journal of Rhinology 2004;18:357–362.

Overton Grant, Nathaniel Bailie, James Watterson, et al. Septal tear in the nose simulation. 2004; 107:1352–1356 in Stud Health Technol Inform.

J. Lindemann; H. J. Brambs; T. Keck; et al. Radical sinus surgery: a numerical study of intranasal airflow. American Journal of Otolaryngology 2005;26:175–180.

J. Lindemann; T. Keck; K. M. Wiesmiller; et al. Computing the inflow and outflow of air via the nose following turbinectomy. 2005;43:24–28. Rhinology.

It was written by Dr. David Wexler, Dr. Robert Segal, and Dr. Jonathan Kimbell. Improving aerodynamic performance by decreasing the number of inferior turbinates using computational fluid dynamics. Reference: Arch Otolaryngol - Head Neck Surg 2005; 131: 1102-1107.

It was concluded by researchers Lee HP, Poh HJ, Chong FH, et al. Airflow pattern changes due to enlarged inferior turbinates: a computational fluid dynamics study. 2009;23:153-158 in the American Journal of Rhinology and Allergy.

Y. Liu, A. M. Edgar, J. J. Gu, et al. In a 2007 issue of J Aerosol Sci., the authors used the Reynolds Averaged Navier-Stokes (RANS), Reynolds Averaged Navier-Stokes (RANS/EIM), and LES numerical methods to simulate aerosol deposition in a three-dimensional human nasal cavity.

Numerical predictions of submicrometer aerosol deposition in the nasal cavity via a new drift flux technique, Xi JX, Longest PW. International Journal of Heat and Mass Transfer. 51 (2008): 5562-5577.

In: Hooper RG, A Quick and Easy Way to Measure Nasal Airflow Using Forced Inspiratory Flow-Volume Curves. 2001 Mayo Clinic Proceedings;76:990-994.

John M. Guilherme, Brian N. Neil, David A. Martins, et al. Nasal cavity air cooling and atrophic rhinitis: a computational fluid dynamics investigation. 2007;103:1082-1092 Journal of Applied Physiology.

Moore E. J. and E. B. Kern. Extensive analysis of 242 instances of atrophic rhinitis. Reference: Am J Rhinol 2001;15:355-361.

Drs. S. Naftali, M. Rosenfeld, M. Wolf, et al. A person's nasal air-conditioning system. 2005, Volume 33, Issue 5: Pages 545–553. Ann. Biomed. Eng.

Drs. S. Grützenmacher, C. Lang, and G. Mlynski. Pre- and post-operative nasal airflow analysis using acoustic and resistivity rhinometry and computational fluid dynamics. Reference: ORL J Otorhinolaryngol Relat Spec. 2003; 65:341-347.

Research by Grützenmacher, Robinson, Grafe, K, et al. Primary results of a model research on airflow in deviated septum nostrils with hypertrophy of the compensatory turbinates. Journal of Otolaryngology – Head and Neck Surgery Supplement. 2006; 68:199-205.

I. Hörschler, To wit: Brücker Ch, Schröder W, et al. Studying how the shape of the nose affects the airflow around it. European Journal of Mechanics B: Fluids, Volume 25, Issue 2 (2006): Pages 471–490.

In: Schroter RC, Watkins NV. Heat transfer during mammalian respiration. 1989;78(2):357-369 in Respir Physiol.

Y. Liu, A. M. Edgar, J. J. Gu, et al. Aerosol deposition in the human nasal cavity simulated numerically using RANS, RANS/EIM, and LES. The citation for this article is J Aerosol Sci 37:683–700 (2007).

Both Xi JX and the Longest PW. Use of an unique drift flux technique to forecast the numerical deposition of submicrometer aerosols in the nasal cavity. International Journal of Heat and Mass Transfer. 51 (2008): 5562-5577.